frontiers in Earth Science

ORIGINAL RESEARCH
published: 12 January 2022
doi: 10.3389/feart.2021.717680

Hydrogeochemistry of Hot Springs and the 2018 Mojiang M 5.9 Earthquake-Related Chemical Changes in the Simao Basin, China

Qilin Li, Ciping Zhao, Yun Wang, Yiying Zhou and Hua Ran*

Yunnan Earthquake Agency, Kunming, China

The Simao Basin is characterized by strong tectonic activity and frequent seismicity. This study investigated the hydrochemical characteristics of 21 thermal springs in the Simao Basin from 2018 to 2020. In this study period, the 2018 Mojiang M5.9 earthquake caused several hydrochemical changes. The results indicate that the Simao Basin contained saline spring waters, HCO_3^--rich spring waters, and SO_4^{2-}-rich spring waters. In the study area, the water chemistry types were controlled by stratum lithology. Saline springs flowed through red beds and dissolved large amounts of halite, which is a rich source of $Cl^-$and Na^+ ions. In the hot spring waters, Ca^{2+} (Mg^{2+}) and HCO_3^- were mainly derived from the dissolution of carbonate minerals, gypsum, and anhydrite of Triassic rocks. The higher SO_4^{2-} content in the hot spring waters was caused by the pyrite present in Ailaoshan metamorphic rocks. The reservoir temperatures (121–289 °C) in the Simao Basin were estimated by the silica-enthalpy mixing model equation and the silica-enthalpy diagram. The hot springs had higher reservoir temperatures (>250 °C) and were mainly located at the edges of the basin. Metamorphic rocks exposed in the region had low permeabilities and these springs was close to nearby deep faults that provided deep heat. In most springs, the concentrations of Ca^{2+} and HCO_3^- ions increased obviously before the 2018 Mojiang M5.9 earthquake; however, the concentrations of these ions decreased after the earthquake. The hydrogeochemical variations might be attributed to the vigorous water-rock interactions and the mixing of secondary fluids. The entry of cold shallow groundwater caused changes in the reservoir temperatures of some spring samples.

Keywords: hot spring, earthquake, hydrochemical characteristics, reservoir temperature, chemical changes

OPEN ACCESS

Edited by:
Zhilei Sun,
Qingdao Institute of Marine Geology (QIMG), China

Reviewed by:
Xianrong Zhang,
Qingdao Institute of Marine Geology (QIMG), China
Zijun Wu,
Tongji University, China

****Correspondence:***
Qilin Li
qilinli1988@163.com

Specialty section:
This article was submitted to Geochemistry, a section of the journal Frontiers in Earth Science

Received: *31 May 2021*
Accepted: *13 December 2021*
Published: *12 January 2022*

Citation:
Li Q, Zhao C, Wang Y, Zhou Y and Ran H (2022) Hydrogeochemistry of Hot Springs and the 2018 Mojiang M 5.9 Earthquake-Related Chemical Changes in the Simao Basin, China. Front. Earth Sci. 9:717680. doi: 10.3389/feart.2021.717680

INTRODUCTION

The Simao Basin (the southern half of the Lanping-Simao Basin) is located in the Yunnan-Tibet Geothermal Belt. It is a typical red-bed basin that exhibits a strong tectonic activity (**Figures 1A,B**). Various types of springs of different sizes exist in the basin. Hot spring is an important part of subsurface fluid and is exposed along fault zone. Therefore, hot spring carries a lot of deep information during migration. The hydrochemical characteristics of hot springs are used to obtain information about geothermal reservoirs and thermal groundwater circulation and may provide insight into potential geothermal resources. In addition, hydrochemical components of spring water are effective indicators of earthquakes, because seismic activity can change the state of underground stress and strain, affect the hydrodynamic conditions and the degree of water-rock

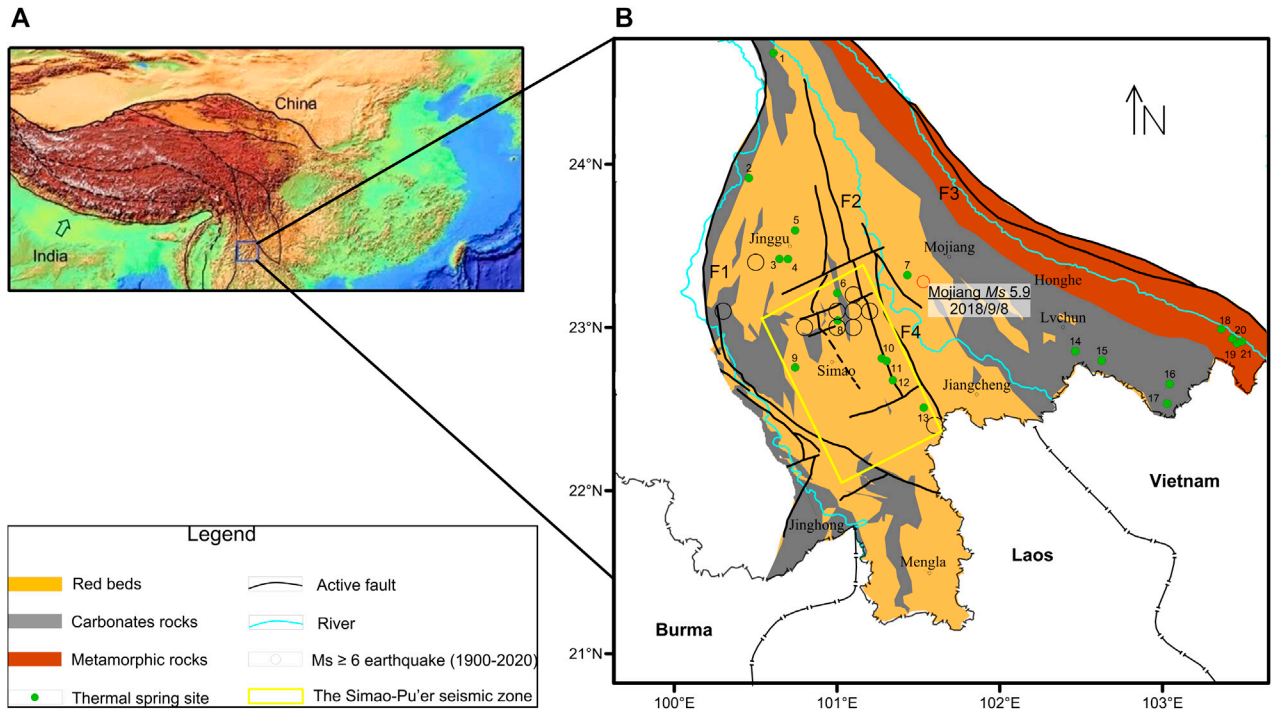

FIGURE 1 | Topographic map of the study area **(A)** and schematic tectonics and spring sites in the Simao Basin **(B)**; modified from Zhang Y. et al., 2020). Abbreviations: F1, Lancangjiang fault; F2, Wuliangshan fault; F3, Ailaoshan fault; F4, Mohei fault.

reaction in the hot spring, and further change the fluid composition and isotope characteristics of hot spring. Some studies on springs in the Simao Basin have focused on potassium exploration through salty and saline springs, the exploration and utilization of geothermal resources, and the origin and evolution of the springs were also examined (Zhang et al., 2013; Bo et al., 2015; Zhang et al., 2018; Zhang L. et al., 2019). However few reports have studied the earthquake-related composition of groundwater characteristics and changes in the basin. The study area is located in the Simao-Pu'er seismic zone, which is one of the most important strong earthquake disaster areas in the Yunnan province (Cheng, 2017). Examination of the hydrochemistry and changes of springs is of great helpful for understanding the breeding process of strong earthquakes in this district.

Earthquake-related groundwater chemical composition changes have been widely used in the search for seismic precursors. Tsunogai and Wakita, 1995 observed increased Cl^- and SO_4^{2-} concentrations in groundwater prior to the Kobe earthquake in Japan. Claesson et al. (2004) observed a rapid increase in multicomponent constituents and a decrease in the Na/Ca content of groundwater due to a seismic event (M = 5.8) in northern Iceland. Changes in the concentrations of Ca^{2+} and HCO_3^- were observed before and after the Wenchuan earthquake (Ms = 8.0), the Lushan earthquake (Ms = 7.0), and the Kangding earthquake (Ms = 6.3) in China (Chen et al., 2015; Li et al., 2019). Seismic hydrochemical changes may be linked to changes in the permeability structure, the mixture of deep and shallow fluids, and/or fluid-rock interactions caused by tectonic activity (Claesson et al., 2004; Zhang X. et al., 2019).

In this study, new hydrochemical data was obtained from the hot springs of Simao Basin. We investigated the hydrochemical characteristics of these thermal springs from 2018 to 2020. During the study period, the 2018 Mojiang M5.9 earthquake occurred in the study area and caused significant hydrochemical changes. Earthquake-related hydrochemical changes were studied and the possible mechanisms in the geothermal area were explained.

GEOLOGICAL SETTING

The Simao Basin is located in southwest Yunnan, China and belongs to the southern section of the Sanjiang fold system, which is narrow in the north and wide in the south in the shape of a broom (**Figures 1A,B**; Yunnan Bureau of Geology and Mineral Resources, 1986). Several huge NW–SE and nearly S–N trending faults control the formation and tectonic evolution of the basin. The Lancangjiang deep fault (F1) in a roughly S–N direction and the Ailaoshan deep fault (F3) in a NW–SE direction are the western and eastern margins of the basin, respectively. A series of NW–SE trending faults are present in the basin, including the Wuliangshan fault (F2) and the Mohei fault (F4) (**Figure 1**; Qu et al., 1998). Most parts of the Simao Basin are underlain by thick Mesozoic and Cenozoic red beds, which mainly contain sandstones and mudstones. Proterozoic metamorphic rocks are only exposed in the margin of the basin. The Upper and Middle Paleozoic limestones outcrop in the central block uplifts and the marginal belt uplifts in the basin (Yunnan Bureau of Geology and Mineral Resources, 1990). According to seismic records, many

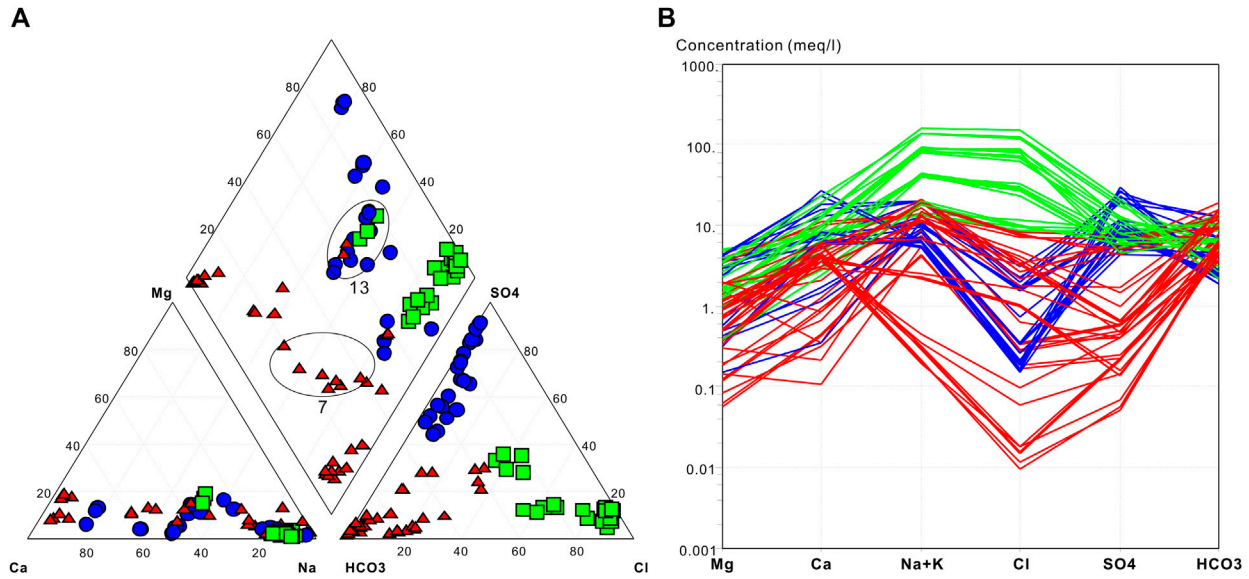

FIGURE 2 | Piper diagram **(A)** and Schoeller diagram **(B)** of the geothermal waters. Process (black circles) indicating the changes before and after the Mojiang earthquake.

moderate and strong crustal earthquakes have occurred in the basin in recent years, including the 2007 Ning'er earthquake (Ms 6.4), the 2014 Jinggu earthquake (Ms 6.6, Ms 5.8, and Ms 5.9), and the 2018 Mojiang earthquake (Ms 5.9) (http://www.ceic.ac.cn/). On September 8, 2018, an Ms 5.9 earthquake occurred at Mojiang, with an epicenter location of 23.28°N, 101.53°E and a focal depth of 11 km. The focal mechanism indicates that the seismogenic, strike-slip fault strikes northeast and dips to the southeast. The strike is between azimuths of 26° and 44°, the dip is between 52° and 71°, and the rake is between 2° and −17° (Zhang Y. et al., 2019). The Simao Basin is situated in the southern Yunnan-Tibet geothermal zone, which shows strong geothermal activity. The active crustal movement creates favourable conditions for the formation of high-temperature geothermal fields (Zhou et al., 2017), which have a terrestrial heat flow of 63.2 MW/m^2 (Xu et al., 1992). The area hosts more than 100 springs. Several types of springs (including hot springs, saline springs and salty springs) exist in the basin (Zhang L. et al., 2019). The temperature and the flow of spring water vary in the dry season and the rainy season, but the water chemistry of springs is stable. Most of the springs emerge in carbonate rocks and water-rich red beds. The distribution of the banded geothermal wells is controlled by the tectonic activities that formed deeper fracture zones, which can provide channels for the enrichment and migration of geothermal fluids.

MATERIALS AND METHODS

Hot springs were geochemically investigated in the Simao Basin from 2018 to 2020, and 38 hydrothermal water samples were obtained (sampling locations shown in **Figure 1B** and **Supplementary Table S1**). A lot of hydrochemical data was collected from previous studies that investigated these thermal spring samples in the 1980s and 2017 (Tong and Zhang, 1994; Zhang X. et al., 2019). The field investigations include on-site measurements of pH, temperature, electrical conductivity (EC), which were measured with a portable multi-parameter water quality analyzer (produced by WTW, Germany). The precision of these factors were 0.01, 0.1°C, and 1 μS cm^{-1}, respectively. Each water sample was filtered on-site with 0.2 μm membranes and was stored in two 250 ml polyethylene bottles. The concentration of major cations (Na^+, K^+, Ca^{2+} and Mg^{2+}) and anions (F^-, Cl^-, NO_2^-, Br^-, $NO_3^-$and SO_4^{2-}) were determined by performing ion chromatography (883 Basic IC plus, Metrohm, Switzerland; detection limit: 0.01 mgL^{-1}) at the Deep-earth fluids Laboratory, Yunnan Earthquake Administration, China. Low concentrations of Li^+, Rb^+, Cs^+, Sr^{2+} were determined with a Thermo Fisher X series II ICP-MS at the Institute of Crustal Dynamics, China Earthquake Administration, Beijing, China. SiO_2 (aq), HCO_3^-, and CO_3^{2-} were detected according to the China National Standard Examination Methods for Drinking Natural Mineral Water (GB/T 8538-2008). SiO_2 (aq) was measured by a visible spectrophotometer, and HCO_3^- and CO_3^{2-} was measured by the volumetric method (HCl titration).

RESULTS AND DISCUSSION

Hydrogeochemistry

The physicochemical parameters and the geochemical data of hot springs in the Simao Basin have been listed in **Supplementary Table S1** and **Supplementary Table S2**. The 21 hot springs had temperatures ranging from 30°C to 102°C. The pH values and total dissolved solids (TDS) were 5.60–8.26 and 237–10,444 mg/L, respectively. The saline spring samples (No. 3, 4, and 5) had

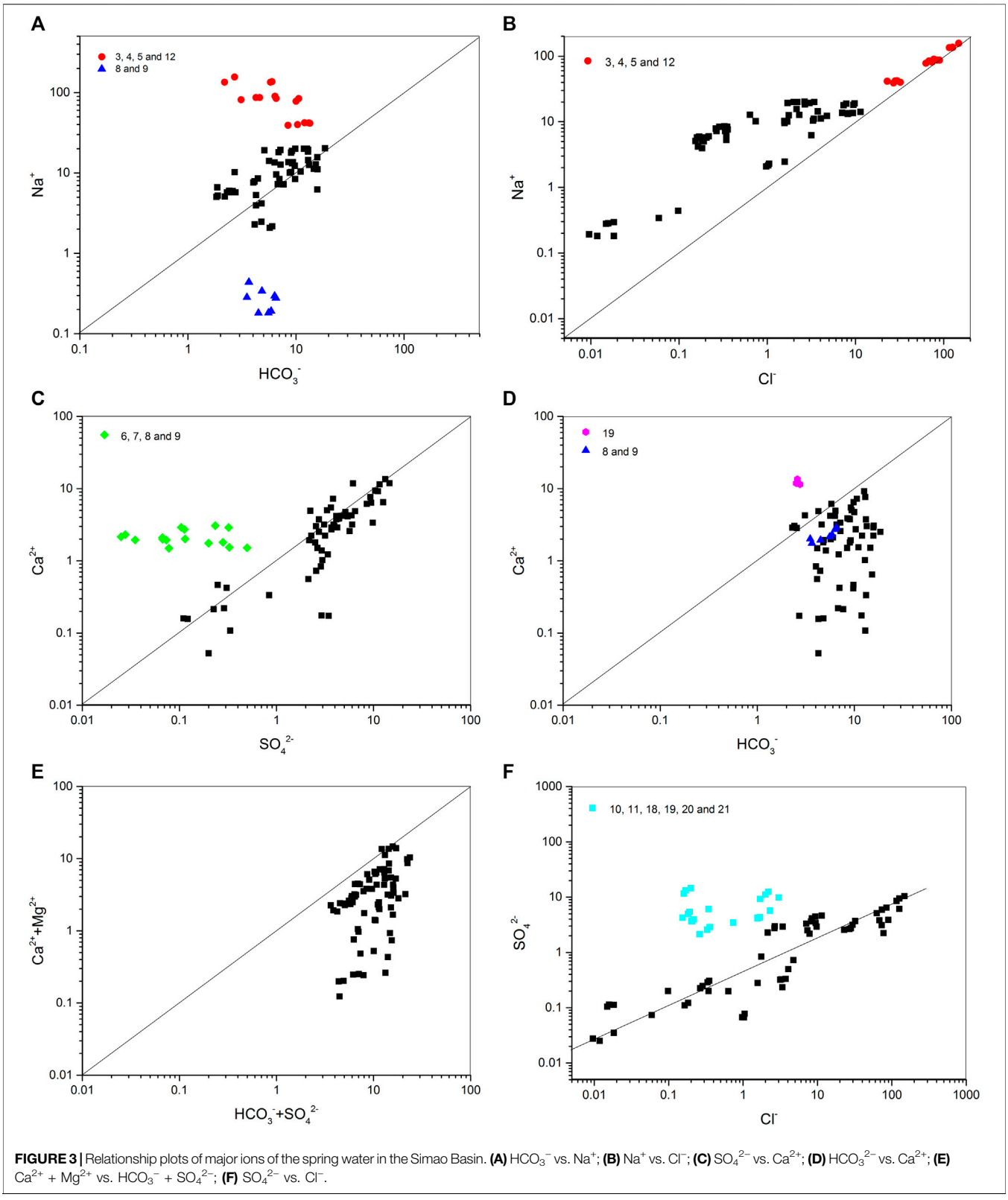

FIGURE 3 | Relationship plots of major ions of the spring water in the Simao Basin. **(A)** HCO_3^- vs. Na^+; **(B)** Na^+ vs. Cl^-; **(C)** SO_4^{2-} vs. Ca^{2+}; **(D)** HCO_3^{2-} vs. Ca^{2+}; **(E)** Ca^{2+} + Mg^{2+} vs. HCO_3^- + SO_4^{2-}; **(F)** SO_4^{2-} vs. Cl^-.

relatively higher TDS values (5,351–10,444 mg/L) than others. The data of ions (K^+, Na^+, Ca^{2+}, Mg^{2+}, Cl^-, SO_4^{2-} and HCO_3^-) was provided from previous studies that investigated the thermal springs from the 1980s to 2020. As shown in **Figure 2**, Piper and Schoeller's diagrams illustrate the concentrations of major and minor ions in springs. In the Piper diagram, the 21 water samples

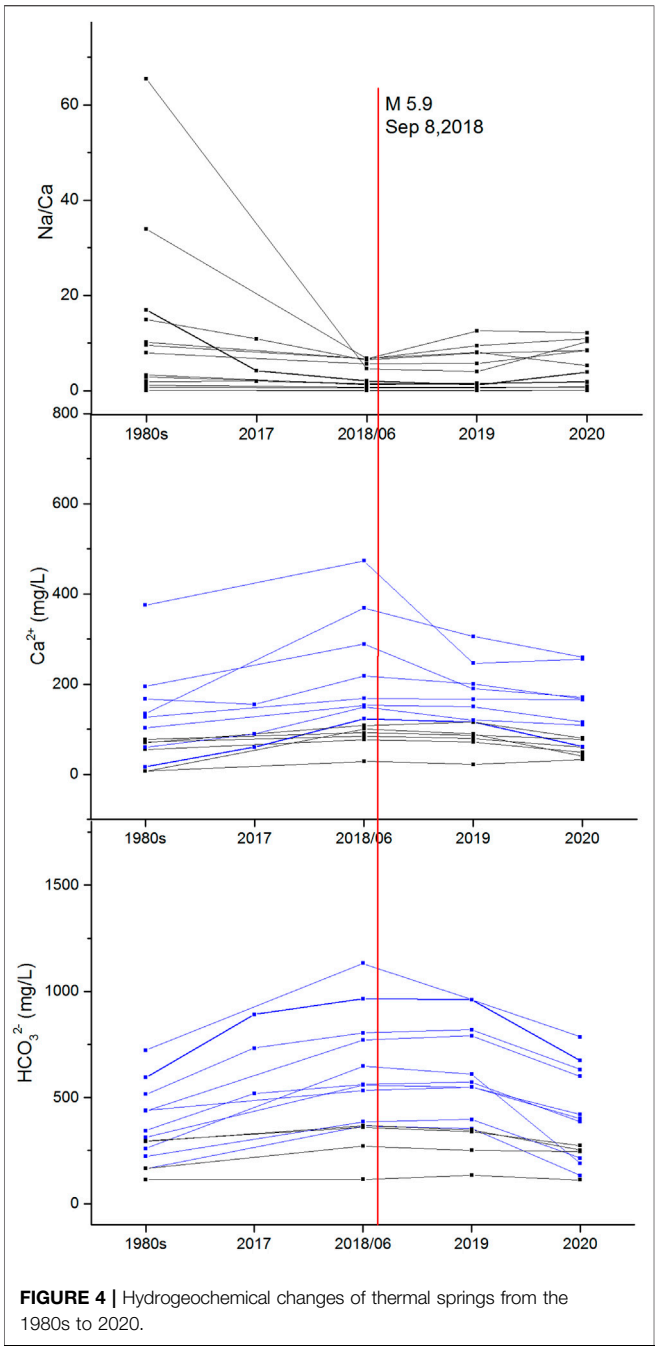

FIGURE 4 | Hydrogeochemical changes of thermal springs from the 1980s to 2020.

have been roughly divided into three groups. Saline spring waters are of Na–Cl type. Samples containing HCO_3^- as the predominant anion ($HCO_3^- > SO_4^{2-} > Cl^-$ or $HCO_3^- > Cl^- > SO_4^{2-}$) include Na-$HCO_3$, Ca-$HCO_3$, Ca-Na-$HCO_3$, Na-Ca-$HCO_3$, Na-$HCO_3$-$SO_4$, Na-$HCO_3$-Cl, Na-Ca-$HCO_3$-$SO_4$, and Na-$HCO_3$-Cl-$SO_4$. Samples containing SO_4^{2-} as the predominant anion ($SO_4^{2-} > HCO_3^- > Cl^-$ or $SO_4^{2-} > Cl^- > HCO_3^-$) include Ca-$SO_4$, Na-Ca-$SO_4$, Ca-Na-$SO_4$, Na-$SO_4$-$HCO_3$, and Na-Ca-$SO_4$-$HCO_3$. Other ions ($Li^+$, NH_4^+, Rb^+, Cs^+, Sr^{2+}, F^-, NO_2^-, Br^-, NO_3^-) were present in relatively low concentrations. In data points 14–21, the components F^- and Sr^{2+} had relatively higher concentrations. This is because F^- and Sr^{2+} were more easily enriched into weak alkaline water, with a pH range of 7.0–8.5 (Cai et al., 2001; Xing et al., 2012).

To understand the origin and the evolution of major ions in thermal groundwater, the relationships between major ions of the spring water were analyzed, i.e. HCO_3^- vs. Na^+, Na^+ vs. Cl^-, SO_4^{2-} vs. Ca^{2+}, HCO_3^{2-} vs. Ca^{2+}, (Ca^{2+} + Mg^{2+}) vs. (HCO_3^- + SO_4^{2-}) and SO_4^{2-} vs. Cl^-, (**Figure 3**). Except for the data points 3, 4, 5, 8, 9, and 12, most of the data points were plotted close to the 1:1 line in **Figure 3A**. This indicated that the quality of Na was affected by the dissolution of Na-feldspar. Samples 8 and 9 are present on the lower-right side of the 1:1 line, which implies that HCO_3^- has another source. **Figure 3D** illustrated that carbonate minerals (calcite and dolomite) were also a source of HCO_3^-. The Triassic carbonate strata in the Simao Basin are located under the Jurassic red bed. The spring water flows through carbonate formations and can dissolve calcite and dolomite. Saline spring waters of data points 3, 4, 5, and 12 have a higher concentration of Na^+ ions and a lower concentration of HCO_3^- ions, with an average molar Na^+/HCO_3^- ratio of 15. This indicates that the dissolution of Na-feldspar is not the main source of these ions (**Figure 3A**). Spring samples of data points 3, 4 and 5 are located in Jinggu County, which is a region with large halite deposits (Yunnan Bureau of Geology and Mineral Resources, 1986). As shown in **Figure 3B**, saline spring samples of data points 3, 4, 5, and 12 contained a high concentration of Cl^- and Na^+ ions, which were present on the dissolution line of NaCl. This indicates that halite is the main source of Na. Except for data points 6, 7, 8, and 9 in the Triassic carbonate rocks, most water falls near the 1:1 line (gypsum dissolution line), suggesting that the dissolution of gypsum and anhydrite is the main source of Ca^{2+} and SO_4^{2-} (**Figure 3C**). In Lanping- Simao Basin, anhydrite is distributed in the thin interlayer of the salt series, and gypsum is distributed in the mud conglomerate layer on the surface (Qu et al., 1998). The ionic ratios of (Ca^{2+} + Mg^{2+}) vs. (HCO_3^- + SO_4^{2-}) in **Figure 3E** show that the dissolution of dolomite, calcite, gypsum, and anhydrite is responsible for the production of Ca^{2+}, Mg^{2+}, SO_4^{2-}, and HCO_3^-. A correlation between Cl^- and SO_4^{2-} can be inferred from **Figure 3F**. The positive chloride-sulfate relation probably reflects the mixing of geothermal water and cold water (Arnórsson, 1985). Atmospheric oxygen in the cold water oxidizes H_2S to SO_4^{2-} at shallow depths (Daniele et al., 2020), which increases the SO_4^{2-} concentration of the geothermal water, (e.g., sampling points 10, 11, 18, 19, 20, and 21). In addition, the lithology suggests that the dissolution of the pyrite-bearing formation rocks near the Ailaoshan fault may increase the SO_4^{2-} content in the groundwater (Luo, 2007). Therefore, the chemical characteristics of geothermal water in the Simao Basin show that the main ions in the hot spring water mainly come from the dissolution of minerals during the circulation of surface water. The water chemistry types are controlled by stratum lithology.

Earthquake-Induced Chemical Variations

As shown in the Piper diagram (**Figure 2**), the water chemistry in No.7 and 13 changed during the study period. Anomalies of the water chemistry types in No. 1 and 2 should not be considered,

TABLE 1 | The estimated reservoir temperatures of hot springs in the Simao Basin.

Sample no	Reservoir temperature (°C)				Sample no	Reservoir temperature (° C)			
	Quartz	Na-K	K-Mg	Na-K-Ca		Quartz	Na-K	K-Mg	Na-K-Ca
1a	91	172	83	176	11a	87	139	52	74
1b	92	129	68	90	11b	85	120	42	48
1c	78	143	70	89	11c	62	119	42	49
1d	91	127	66	128	11d	55	120	41	51
2a	116	151	83	144	12a	102	108	73	121
2b	117	100	68	75	12aa	85	149	92	151
2c	111	115	74	83	12b	111	92	70	90
2d	116	101	68	83	12c	100	86	69	90
3b	85	84	77	105	12d	100	87	70	91
3c	83	78	79	101	13a	91	115	42	56
3d	81	78	79	102	13aa	74	114	40	55
4a	97	101	81	118	13b	85	86	33	33
4b	100	71	66	90	13c	77	86	32	36
4c	67	63	67	86	13d	82	84	31	38
4d	95	63	67	87	14a	117	202	106	197
5a	91	97	91	118	14c	111	180	102	164
5b	88	71	75	94	14d	103	170	97	162
5c	86	67	83	94	15c	138	166	97	153
5d	92	67	82	94	15d	124	166	96	153
6a	83	157	38	28	16a	134	224	96	200
6b	82	142	33	17	16c	128	201	89	170
6c	63	142	33	16	16d	124	204	89	171
6d	77	136	32	21	17c	134	186	98	163
7a	107	207	79	185	17d	125	187	99	165
7aa	99	194	79	164	18a	146	205	75	72
7b	111	193	73	91	18b	138	190	68	51
7c	91	248	83	87	18c	120	190	67	51
7d	104	195	72	163	18d	128	189	67	50
8a	69	191	12	109	19b	133	223	65	46
8b	62	258	14	131	19c	99	215	55	45
8c	51	260	14	131	19d	130	214	55	44
8d	79	255	13	130	20b	162	222	88	75
9a	57	94	-	59	20c	149	223	87	75
9b	48	195	15	107	20d	156	223	87	75
9c	32	198	15	107	21a	177	216	111	196
9d	67	200	16	111	21b	164	221	91	182
10a	102	168	70	149	21c	154	221	92	183
10b	100	139	66	67	21d	153	223	91	180
10c	74	139	58	69					
10d	88	140	59	74					

because the epicentral distance of these two anomalous sites is far above the theoretical distance influenced by the quake with magnitude (M) 5. No.7 is located in the near-field of the Mojiang earthquake. The water chemistry in No.7 changed from Na-HCO_3-Cl to Na-Ca-HCO_3 in June 2018 before the Mojiang M5.9 earthquake on September 8 and from Na-Ca-HCO_3 back to Na-HCO_3-Cl in 2020. Similarly, the water chemistry in No.13 changed from Na-Ca-Cl-SO_4-HCO_3 to Na-Ca-HCO_3-Cl-SO_4 before the Mojiang M5.9 earthquake and from Na-Ca-HCO_3-Cl-SO_4 back to Na-Ca-Cl-SO_4-HCO_3 after the earthquake; however, no significant changes were observed in other spring samples (**Supplementary Table S1**). For these spring samples, the time series of anion and cation ions for these springs were plotted (**Figure 4**). Based on previous case studies documenting hydrogeochemical response to seismicity, the groundwater chemistry fluctuates due to rainfall and other superficial phenomena. During the entire sampling period, most of the cations and anions varied with the two sigma relative standard deviation (2σ). Before the earthquake, ionic concentration increased slightly (only 10–20% above the background value) and was considered insignificant (Toutain et al., 1997; Li et al., 2021). In the springs, Ca^{2+} and HCO_3^- ions exhibited significant changes before the Mojiang M5.9 earthquake; however, other ions stayed relatively stable in the springs. In most springs (blue lines), the concentration of Ca^{2+} and HCO_3^- ions increased obviously (about 28–77% above the background value) before the Mojiang M5.9 earthquake; however, it decreased after the earthquake (**Figure 4**). The data points 6, 8, 9, 18, 19, 20, and 21 (black lines) changed slightly before and after the earthquake. The Na/Ca ratio appeared to be sensitive to changing stresses, which were associated with M > 4 earthquakes (Claesson et al., 2004). In **Figure 4**, the Na/Ca data decreased before the Mojiang M5.9 earthquake. After the earthquake, the Na/Ca ratio increased slightly and then recovered in 2020.

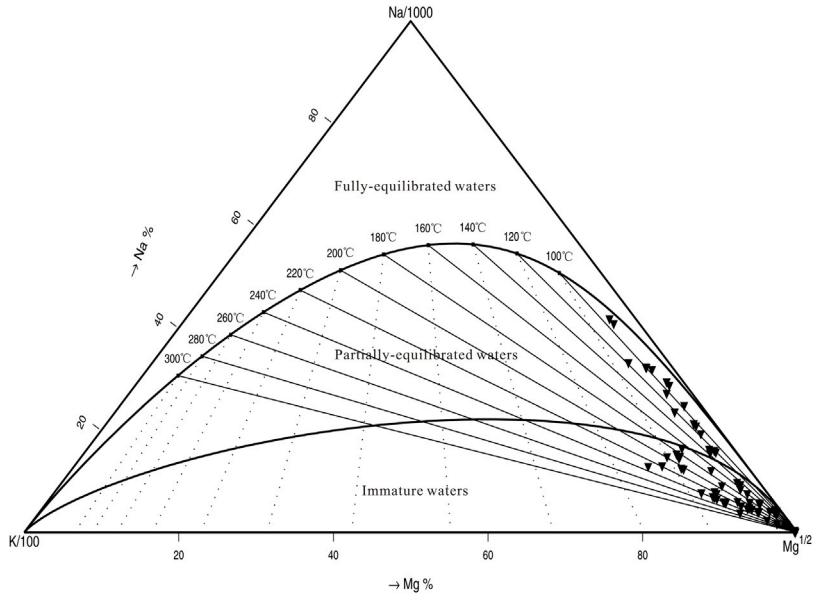

FIGURE 5 | The Na-K-Mg trilinear equilibrium diagram of hydrothermal water of the Simao Basin.

Reservoir Temperature and Variations

Reservoir temperature is an important parameter, which is used for classifying the genetic types of geothermal systems. Moreover, it is also used for evaluating the geothermal potential of geothermal fields, which can be estimated with geochemical geothermometers. The concentration of solutes in geothermal fluids is a function of the geothermal reservoir temperature. In theory, all chemical reactions controlled by temperature can be used as geochemical geothermometers (Ellis, 1970; Wang et al., 1993).

Traditionally, the cation ratio geothermometers such as Na-K, Na-K-Ca, and K-Mg geothermometers and SiO_2 geothermometers were used to estimate the geothermal reservoir temperature (Fournier, 1981; Giggenbach, 1988; Verma and Santoyo, 1997). As shown in **Table 1**, the reservoir temperatures were calculated by using **Eqs 1–4**.

$$\theta_{\text{quartz}}\,(^{\circ}\text{C}) = \frac{1309}{5.19 - \log\,(SiO_2)} - 273.15 \tag{1}$$

$$\theta_{\text{NaK}}\,(^{\circ}\text{C}) = \frac{1217}{1.483 - \log\frac{(\text{Na})}{\text{K}}} - 273.15 \tag{2}$$

$$\theta_{\text{NaKCa}}\,(^{\circ}\text{C}) = \frac{1647}{\log\frac{(\text{Na})}{\text{K}} + \beta\,(\log(\sqrt{Ca}/Na) + 2.06) + 2.47} - 273.15 \tag{3}$$

$$\theta_{\text{KMg}}\,(^{\circ}\text{C}) = \frac{4410}{14.0 - \log\left[\frac{\text{K}^2}{\text{Mg}}\right]} - 273.15 \tag{4}$$

As shown in **Table 1**, the reservoir temperatures calculated by quartz geothermometers were in the range of 32–177°C, and those calculated by cation geothermometers were as follows: 63–260°C (Na-K), 12–91°C (Na-K) and 16-200 (Na-K-Ca), respectively. The Na-K-Mg triangular diagram classified spring waters into three types: fully-equilibrated waters, partially-equilibrated waters and immature waters. These water types were used to determine whether a fluid reached water-rock equilibrium (Giggenbach, 1988). Only fully-equilibrated waters could be used with cation geothermometers. In **Figure 5**, most data points were in the area of immature water, which was present in the hot springs plot. Sample No. 2, 3, 4, 5, and 12 were located in the partially-equilibrated area of the triangular diagram. This indicates that the wall rock have not reached equilibrium due to the addition of a significant quantity of cold water (shallow groundwater). This implies that cation geothermometers are not suitable for calculating the reservoir temperatures of the study area.

The reservoir temperature in the Simao Basin was calculated by Zhang Y. et al., 2019. Their study indicates that compared to cation geothermometers, quartz geothermometer provides more reasonable estimations of the reservoir temperature of this area (Zhang L. et al., 2019). As mentioned previously, the studied hot spring waters are mixtures of thermal groundwater and shallow cold waters, which cause a high dilution of silica concentration. Therefore, the temperatures calculated with SiO_2 geothermometers (**Table 1**) were lower than the most reliable reservoir temperatures. The silica-enthalpy mixing model equation and the silica-enthalpy diagram can be used to estimate the proportion of thermal groundwater and cold waters. Moreover, they can be used to measure the original temperature of the thermal groundwater component, which can be further considered as the reservoir temperature (Fournier, 1977). The proportion of cold water during mixing was calculated by the following silica-enthalpy **Eqs 5**, **6** (Fournier et al., 1974).

$$\text{H}_\text{c} \cdot \text{X}_1 + \text{H}_\text{h}\,(1 - \text{X}_1) = \text{H}_\text{s} \tag{5}$$

$$\text{Si}_\text{c} \cdot \text{X}_2 + \text{Si}_\text{h}\,(1 - \text{X}_2) = \text{Si}_\text{s} \tag{6}$$

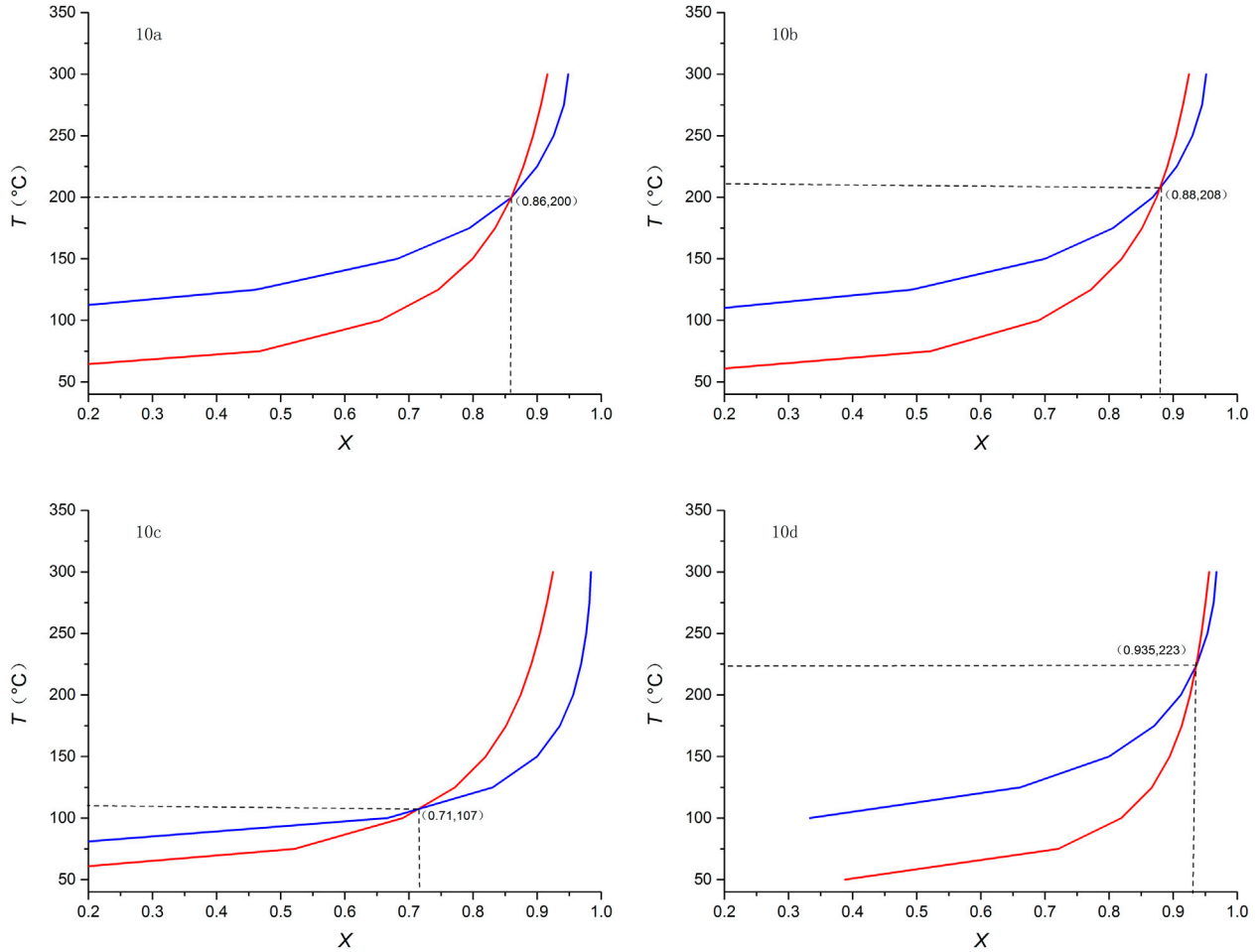

FIGURE 6 | A diagram of temperature relative to the proportion of cold water in hot spring sample 10 (*X* is the proportion of the cold water).

where H_c is the enthalpy of the near-surface cold water, H_h is the initial enthalpy of deep hot water, and H_s is the enthalpy of mixed hot water. Moreover, Si_c is the silica content of near-surface cold water, Si_h is the initial silica content of deep hot water, and Si_s is the silica content of mixed hot water. X_1 and X_2 are the calculated cold water mixing ratios of enthalpy and the SiO_2 concentration, respectively. The solution of **Eqs 5**, **6** was calculated by using a diagrammatic method (**Figure 6**, taking the example of samples 10a-d) because the values of X_1, X_2, and H_s are unknown. The relationship between *X* and temperature was plotted to obtain two curves, whose intersection indicated the estimated proportion of cold water and the original temperature of the thermal groundwater component. The silica-enthalpy diagram is another way to estimate the temperature of the deep thermal groundwater, by using a plot of silica concentration vs. the enthalpy of water (Fournier, 1977). A line passed through the characteristic points of cold (point A) and geothermal (point B) waters; the intersection of the line is point C. The quartz solubility curve illustrates the enthalpy of the deep thermal groundwater (**Figure 7**, taking the example of samples 10a-d).

Except for the data points 4c, 5c, 7c, 10c, and 12c at abnormal lower temperatures, the reservoir temperatures of the mixing model of the silica-enthalpy equation and diagram were in the range of 121°C and 289°C (**Table 2**). As shown in **Table 2**, these values were significantly higher than those of reservoir temperatures, which were determined by the SiO_2 geothermometer. The proportions for cold water ranged from 69 to 98%. An intersection point was not obtained at the plots of samples 1c-d, 6c, 8c, 9a-d, 11c, 14a-d, 16a-d, 18a-d, and 19a-d. This indicates that heat was lost before mixing the hot and cold waters. The existence of the low-velocity zones (LVZs) has been revealed by seismic imaging beneath the Simao Basin within the middle-lower crust at a depth of 15–30 km, and is considered to be possible ductile crustal flow (Bai et al., 2010; Bao et al., 2015; Li et al., 2016). The ductile crustal flow may be a dominant heat source of hot springs in the Simao Basin. The hot springs had higher reservoir temperatures (>250°C) and were mainly located at the margin of the Simao basin, that is, sample sites 2, 13, 15, 17, 20, and 21. At this location, the Lancangjiang and Ailaoshan deep faults were well-developed. A fracture is the main channel for hot water circulation, and the deep faults help provide deep heat for the spring waters (Tang et al., 2017). In the study area, the fissures were well-developed in carbonate rocks. However, the metamorphic

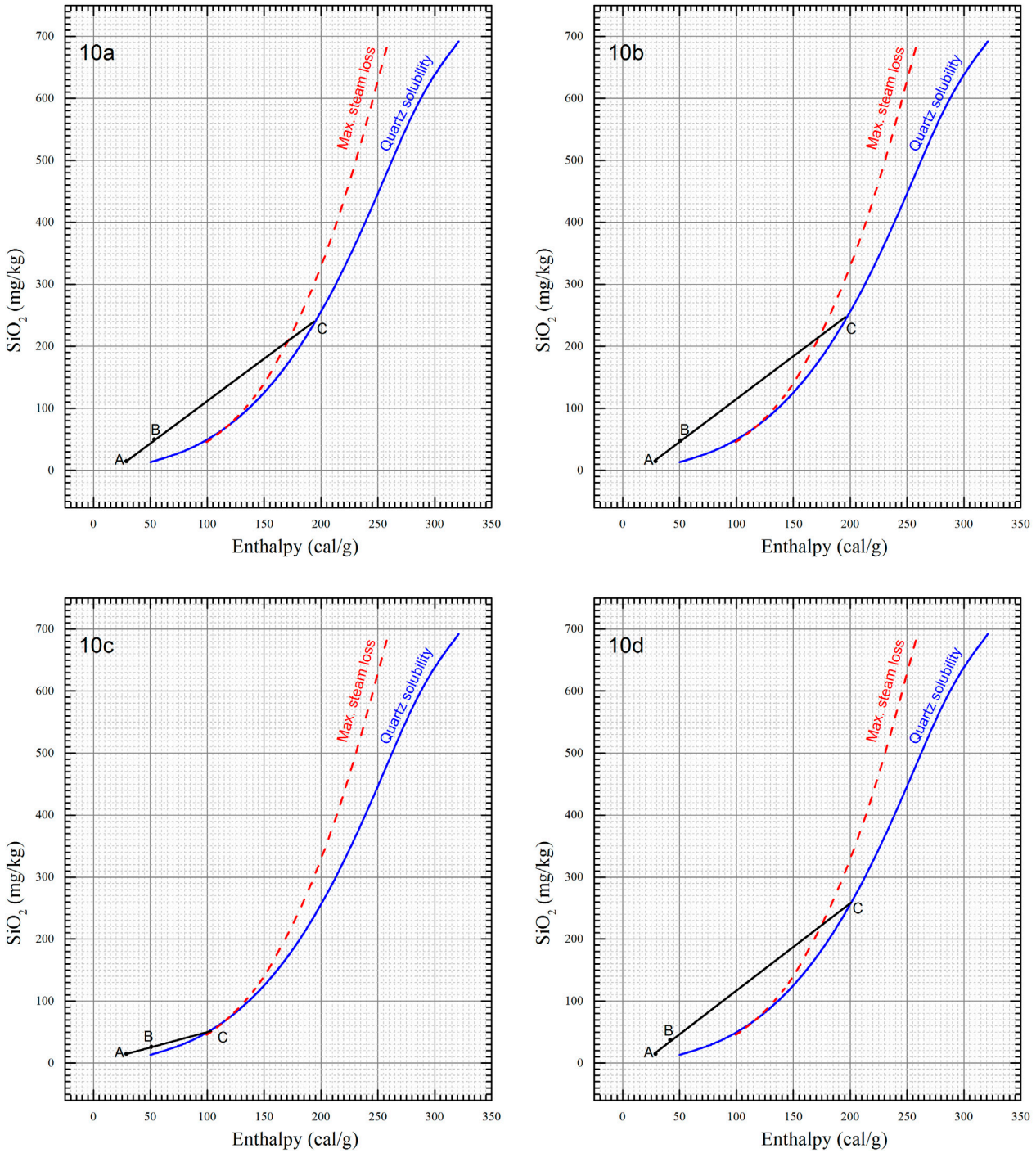

FIGURE 7 | The silica-enthalpy diagram of hot spring sample 10.

strata were exposed in the margin of the basin, which seemed to have low permeability. As a result, springs that emerged in the Ailaoshan metamorphic rocks had higher reservoir temperatures.

The sampling points 4c, 5c, 7c, 10c, and 12c, which were located at about 50–150 km away from the epicentre of the M5.9 Mojiang earthquake. After the earthquake, these reservoir temperatures showed a massive decline (**Figure 8**). In particular, the reservoir temperatures of the sample 10c decreased by about 100°C after the M5.9 Mojiang earthquake; however, the reservoir temperature of the sample 10c recovered in the year 2020 (200–223°C). The variations in reservoir temperature were similar to those observed after the M 8.0 Wenchuan earthquake (Li et al., 2019). The reservoir temperature was approximately 340°C before the Wenchuan

TABLE 2 | Reservoir temperatures based on the silica-enthalpy mixing model and cold water mixing proportions of the hot springs in the Simao Basin.

Sample	Reservoir temperature (° C)		Cold water mixing proportion (%)	Sample	Reservoir temperature (° C)		Cold water mixing proportion (%)
	Silica-enthalpy graph	Silica-enthalpy equation			Silica-enthalpy graph	Silica-enthalpy equation	
1a	226	220	92.6	11a	231	234	94.6
1b	192	194	89	11b	231	228	94.7
1c	—	—	—	11c			
1d	—	—	—	11d			
2a	280	275	91.3	12a	225	218	88.9
2b	—	—	—	12aa	225	219	94
2c	272	263	91.5	12b	227	225	87
2d	—	—	—	12c	188↓	192↓	84.7
3b	241	258	96.2	12d	200	216	89.2
3c	—	—	—	13a	256	247	94.7
3d	—	—	—	13aa	146	154	90.6
4a	214	203	88.5	13b	—	—	—-
4b	194	194	85.3	13c	279	263	97.6
4c	103↓	107↓	81.7	13d	—	—	—
4d	193	193	87.2	14a	—	—	—
5a	147	148	76.9	14c	—	—	—
5b	142	140	74.7	14d	—	—	—
5c	114↓	129↓	71.4	15c	252	246	80.9
5d	150	150	77.2	15d	208	206	76
6a	143	151	84	16a	—	—	—
6b	140	149	83.8	16c	—	—	—
6c	—	—	—	16d	—	—	—
6d	121	126	80.3	17c	268	267	85.6
7a	185	184	78.5	17d	239	233	82.7
7aa	154	150	69.2	18a	—	—	—
7b	187	190	78.2	18b	—	—	—
7c	122↓	122↓	59.3	18c	—	—	—
7d	165	171	76.2	18d	—	—	—
8a	225	256	98.4	19b	—	—	—
8b	217	183	97.9	19c	—	—	—
8c	—	—	—	19d	—	—	—
8d	—	—	—	20b	—	—	—
9a	—	—	—	20c	289	271	81.2
9b	—	—	—	20d	—	—	—
9c	—	—	—	21a	—	—	—
9d	—	—	—	21b	278	263	73.5
10a	190	200	85.9	21c	250	235	69.4
10b	197	208	87.9	21d	246	237	71.1
10c	105↓	107↓	71.3				
10d	200	223	93.5				

earthquake, and it decreased to a relatively stable level after the earthquake (220–260°C).

THE ASSUMPTIONS OF EARTHQUAKE-RELATED HYDROGEOCHEMICAL VARIATION

Two assumptions have often been used to explain earthquake-related hydrogeochemical changes (Claesson et al., 2007): 1) hydrogeochemical shifts record accelerated water-rock interactions resulting from an increased reactive surface area caused by fracture of the sampled aquifer; or 2) hydrogeochemical shifts record the mixing of (or switching between) chemically distinct aquifers. This could occur in response to the fracture of a hydrological barrier between aquifers or because of a change in the relative pressures of connected aquifers.

Whenever an earthquake occurs, the pore pressure of rocks is enhanced. Since a seismic wave propagates through the rocks, it causes an extensive fracture of the wall rock (Du et al., 2013). This increases the rock's surface area, which is in contact with groundwater. Thus, the water-rock interactions become more intensive. In hydrogeochemistry, the saturation index (SI) is commonly used to indicate the chemical states of the mineral phases of groundwater. The saturation state of hot springs in the Simao Basin was calculated based on the chemical compositions and physicochemical parameters of the hydrothermal waters *via* the PHREEQC program package (Parkhurst and Appelo, 1999). All the samples were undersaturated with gypsum, anhydrite, celestite and halite (SI < 0), showing no obvious changes before and after the Mojiang earthquake. However, the SI values of carbonate minerals (calcite and aragonite) exhibited significant changes before and after the earthquake. **Figure 9** illustrates the saturation trends of calcite and aragonite. The SI values of calcite

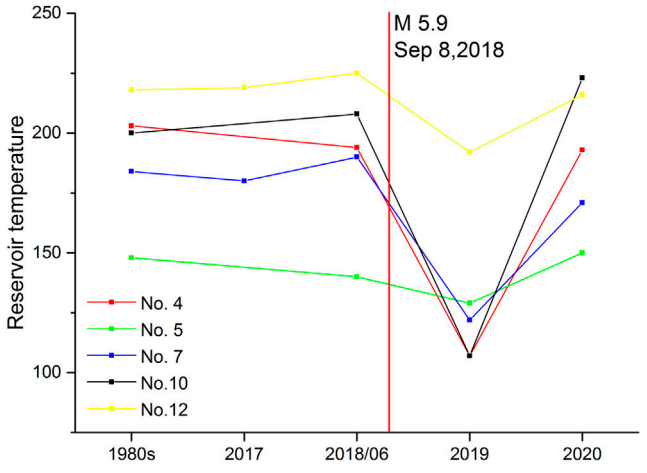

FIGURE 8 | Reservoir temperature variations in some springs from the 1980s to 2020.

and aragonite in almost all undersaturated sampling points reached saturation before the Mojiang M5.9 earthquake, indicating the enhanced dissolution of carbonate rocks. Thus, the increases in the concentrations of Ca^{2+} and HCO_3^- ions were observed during the Mojiang earthquake. The water chemistry of No.7 and No.13 sites changed from Na-HCO_3-Cl to Na-Ca-HCO_3, and from Na-Ca-Cl-SO_4-HCO_3 to Na-Ca-HCO_3-Cl-SO_4, respectively. This also indicates that the dissolution of Ca^{2+} and HCO_3^- ions were in progress. After the earthquake, the SI ratios continued to increase and reached oversaturated levels. This implies that precipitation occurred in the hot springs of the Simao Basin, and the concentration of dissolved ions decreased. The SI values decreased and recovered in 2020. This progressive re-equilibration was possible due to water-rock interactions, which explains why the concentration of Ca^{2+} and HCO_3^- ions decreased to their pre-seismic levels. Moreover, the water chemistry of No.7 and No.13 sites also recovered. Although the vigorous water-interaction model is used to explain the changes in the chemical components (i.e., major and trace elements) following an earthquake, the model fails to explain the variables that indicate water mixing or interactions with deep fluids (e.g., water isotopes, dissolved gases and reservoir temperature; Binda et al., 2020).

The rupture of hydrological barriers or permeability changes are probable causes of variations in ionic concentrations and reservoir temperature. Seismic waves may enhance the permeability of the affected aquifers through increasing fracture porosity, changing pore pressure, and fracturing aquitards. These seismic effects could result in the mixing of fluids from different aquifers or the upwelling of deep fluids (Binda et al., 2020). Before the occurrence of the Mojiang earthquake (from April to July 2018), the compressive activity was significantly greater around the Jingdong-Simao region (Yang et al., 2019). A compressional setting favored an increase in pore pressure induced in Moderate shocks (De Gregorio et al., 2012). Under the N–S-trending tectonic compression stresses, the local stress concentration may cause a new fracture and induce moderate to strong earthquakes like the Mojiang M5.9 earthquake (Chang et al., 2019). New fractures were created during the Mojiang earthquake, which caused the permeability to increase greatly. The obvious increases in the concentrations of Ca^{2+} and HCO_3^- may be attributed to a secondary fluid, which is rich in Ca^{2+} and HCO_3^- ions and originates from the underlying carbonate strata. In addition, the variation in ionic concentrations may be correlated to the contribution of deep fluids. Under the Simao-Pu'er seismic zone, strong low-velocity zones are visible, suggesting the existence of an upwelling asthenosphere in the uppermost mantle (Li et al., 2016; Zhang Z. et al., 2020). Deep degassing results indicate that high He isotopes signatures ($^3He/^4He$ = 5.75–8.36 Ra; mantle-derived He >70%) are present in this region (Zhao et al., 2018). An increased $^3He/^4He$ ratios were observed in the hot springs before the occurrence of M > 4 earthquakes in the Simao-Pu'er seismic zone. This implies that much deeper fluid was added to these springs. Moreover, a similar phenomenon that caused changes in the reservoir temperature

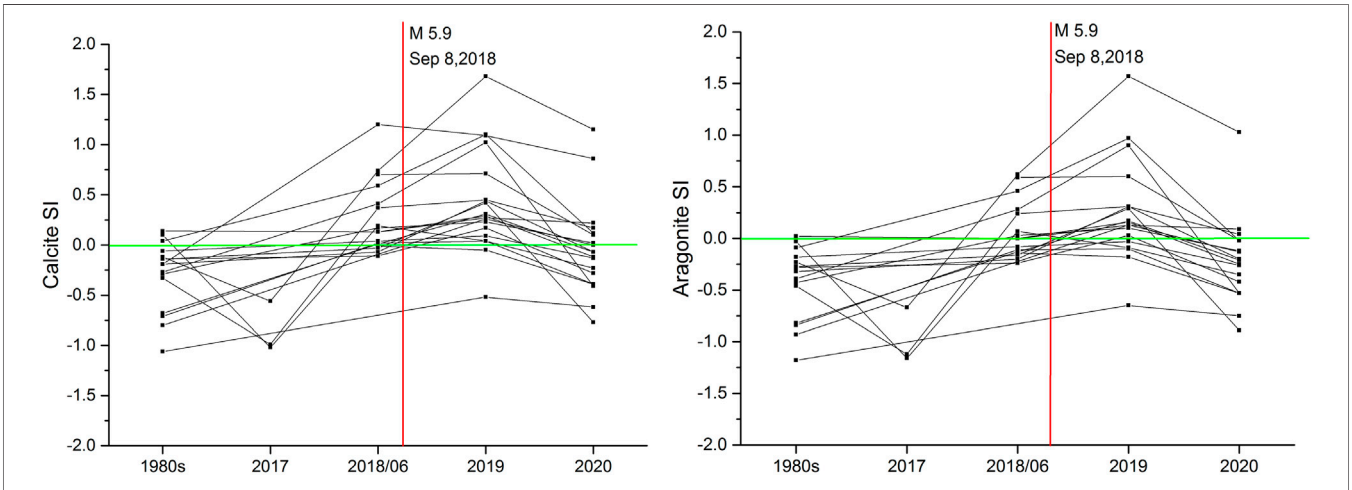

FIGURE 9 | Variations in the SIs of calcite and aragonite in the hot springs from the 1980s to 2020.

was the M 8.0 Wenchuan earthquake (Li et al., 2019). Variations in reservoir temperature after the Mojiang earthquake may have been caused by the entrance of cold shallow groundwater into the reservoir, which participated in deep circulation; however, the clogging of fractures prevented the entry of shallow cold groundwater, and the reservoir temperature increased. Thus, we infer that the chemical changes that occurred after the Mojiang earthquake were caused by the mixing of fluids and water-rock interaction.

CONCLUSION

From 2018 to 2020, the hydrochemical characteristics of 21 thermal springs of the Simao Basin were determined. These water samples were roughly divided into three groups: saline spring waters, HCO_3^--rich spring waters, and SO_4^{2-}-rich spring waters. In the study area, the water chemistry types were controlled by stratum lithology. Ca^{2+} (Mg^{2+}) and HCO_3^- in the hot spring waters were mainly derived from the dissolution of carbonate minerals, gypsum, and anhydrite in Triassic rocks. The saline springs flowed in the red beds and dissolved a large amount of halite with high Cl^- and Na^+ contents. The Ailaoshan metamorphic rocks contain pyrite, which may increase the SO_4^{2-} content in the hot spring waters. The reservoir temperatures (121–289°C) of the Simao Basin were determined. It is speculated that the ductile crustal flow could be the dominant heat source of the hot springs of Simao Basin. The hot springs had higher reservoir temperatures (>250°C) and were mainly located at the edges of the basin. Metamorphic rocks exposed in the region had low permeabilities and these springs was close to nearby deep faults that provided deep heat.

During the study period, the 2018 Mojiang M5.9 earthquake occurred in the study area and caused significant hydrochemical changes. The concentrations of Ca^{2+} and HCO_3^- ions increased obviously in most springs, just before the occurrence of the Mojiang M5.9 earthquake; however, the concentrations of these ions decreased after the earthquake. The hydrogeochemical variation might be attributed to the vigorous water-rock interactions and the mixing of a second fluid. The reservoir temperature decreased after the earthquake. This may have been caused by the entry of cold shallow groundwater.

DATA AVAILABILITY STATEMENT

The original contributions presented in the study are included in the article/**Supplementary Material**, further inquiries can be directed to the corresponding author.

AUTHOR CONTRIBUTIONS

QL: Conceptualization, Investigation, Writing—original draft, Visualization. CZ: Methodology, Data curation. YW: Investigation, Discussion. YZ and HR: Investigation.

FUNDING

This study was supported by the project of Science for Earthquake Resilience of China (XH20053Y) and the Special Fund of the Institute of Earthquake Forecasting, China Earthquake Administration (2017IES010205).

ACKNOWLEDGMENTS

We sincerely thank the reviewers and the editor for providing useful comments and suggestions, which greatly improved the quality of this manuscript.

SUPPLEMENTARY MATERIAL

The Supplementary Material for this article can be found online at: https://www.frontiersin.org/articles/10.3389/feart.2021.717680/full#supplementary-material

REFERENCES

Bai, D., Unsworth, M. J., Meju, M. A., Ma, X., Teng, J., Kong, X., et al. (2010). Crustal Deformation of the Eastern Tibetan Plateau Revealed by Magnetotelluric Imaging. *Nat. Geosci* 3, 358–362. doi:10.1038/ngeo830

Bao, X., Sun, X., Xu, M., Eaton, D. W., Song, X., Wang, L., et al. (2015). Two Crustal Low-Velocity Channels beneath SE Tibet Revealed by Joint Inversion of Rayleigh Wave Dispersion and Receiver Functions. *Earth Planet. Sci. Lett.* 415, 16–24. doi:10.1016/j.epsl.2015.01.020

Binda, G., Pozzi, A., Michetti, A. M., Noble, P. J., and Rosen, M. R. (2020). Towards the Understanding of Hydrogeochemical Seismic Responses in Karst Aquifers: A Retrospective Meta-Analysis Focused on the Apennines (Italy). *Minerals* 10, 1058. doi:10.3390/min10121058

Bo, Y., Liu, C., Zhao, Y., and Wang, L. (2015). Chemical and Isotopic Characteristics and Origin of spring Waters in the Lanping-Simao Basin, Yunnan, Southwestern China. *Geochemistry* 75, 287–300. doi:10.1016/j.chemer.2015.04.002

Cai, C., Franks, S. G., and Aagaard, P. (2001). Origin and Migration of Brines from Paleozoic Strata in Central Tarim, China: Constraints from 87Sr/86Sr, δD, δ18O and Water Chemistry. *Appl. Geochem.* 16, 1269–1284. doi:10.1016/s0883-2927(01)00006-3

Chang, Z. F., Mao, Z. B., Ma, B. Q., and Dai, B. Y. (2019). The Amojiang Fault Zone and Mojiang M5.9 Earthquake in 2018 in Southern Yunnan Province. *Geol. Bull. China* 38, 967–976. doi:10.1007/s11631-019-00352-y

Chen, Z., Zhou, X., Du, J., Xie, C., Liu, L., Li, Y., et al. (2015). Hydrochemical Characteristics of Hot spring Waters in the Kangding District Related to the Lushan MS = 7.0 Earthquake in Sichuan, China. *Nat. Hazards Earth Syst. Sci.* 15, 1149–1156. doi:10.5194/nhess-15-1149-2015

Cheng, Y. (2017). The Characteristics and Tectonic Implications of Electrical Structure beneath the Pu'er Area (In Chinese). *Recent Dev. World Seismol* 12, 1–23.

Claesson, L., Skelton, A., Graham, C., Dietl, C., Mörth, M., Torssander, P., et al. (2004). Hydrogeochemical Changes before and after a Major Earthquake. *Geol* 32, 641–644. doi:10.1130/g20542.1

Claesson, L., Skelton, A., Graham, C., and Mörth, C.-M. (2007). The Timescale and Mechanisms of Fault Sealing and Water-Rock Interaction after an Earthquake. *Geofluids* 7, 427–440. doi:10.1111/j.1468-8123.2007.00197.x

Daniele, L., Taucare, M., Viguier, B., Arancibia, G., Aravena, D., Roquer, T., et al. (2020). Exploring the Shallow Geothermal Resources in the Chilean Southern

Volcanic Zone: Insight from the Liquiñe thermal Springs. *J. Geochemical Exploration* 218, 106611. doi:10.1016/j.gexplo.2020.106611

De Gregorio, S., Federico, C., Cappuzzo, S., Favara, R., Giudice, G., Gurrieri, S., et al. (2012). Stress-induced Temperature Variations in Groundwater of the Monferrato Area (North-Western Italy). *Geofluids* 12, 142–149. doi:10.1111/j.1468-8123.2011.00348.x

Du, J., Zhou, X., Chen, Z., Cui, Y., Liu, L., Li, Y., et al. (2013). Responses of Mud Volcanoes in the North Tianshan to the 30 June 2012 Xinyuan-Hejing MS 6.6 Earthquake. *Acta Seismol Sin* 35, 876–887. doi:10.3969/j.issn.0253-3782.2013.06.011

Ellis, A. J. (1970). Quantitative Interpretation of Chemical Characteristics of Hydrothermal Systems. *Geothermics* 2, 516–528. doi:10.1016/0375-6505(70)90050-7

Fournier, R. O. (1981). "Application of Water Geochemistry to Geothermal Exploration and Reservoir Engineering," in *Geothermal Systems: Principles and Case Histories* (New York: Jonh Wiley and Sons Ltd), 109–143.

Fournier, R. O. (1977). Chemical Geothermometers and Mixing Models for Geothermal Systems. *Geothermics* 5, 41–50. doi:10.1016/0375-6505(77)90007-4

Fournier, R. O., Truesdell, A. H., and Calif, M. P. (1974). Geochemical Indicators of Subsurface Temperature-Part 2, Estimation of Temperature and Fraction of Hot Water Mixed with Cold Water. *Jour. Res. U.S. Geol. Surv.* 2, 263–270.

Giggenbach, W. F. (1988). Geothermal Solute Equilibria. Derivation of Na-K-Mg-Ca Geoindicators. *Geochimica et Cosmochimica Acta* 52, 2749–2765. doi:10.1016/0016-7037(88)90143-3

Li, B., Shi, Z., Wang, G., and Liu, C. (2019). Earthquake-related Hydrochemical Changes in thermal Springs in the Xianshuihe Fault Zone, Western China. *J. Hydrol.* 579, 124175. doi:10.1016/j.jhydrol.2019.124175

Li, C., Zhou, X., Yan, Y., Ouyang, S., and Liu, F. (2021). Hydrogeochemical Characteristics of Hot Springs and Their Short-Term Seismic Precursor Anomalies along the Xiaojiang Fault Zone, Southeast Tibet Plateau. *Water* 13, 2638. doi:10.3390/w13192638

Li, M., Zhang, S., Wang, F., Wu, T., and Qin, W. (2016). Crustal and Upper-Mantle Structure of the southeastern Tibetan Plateau from Joint Analysis of Surface Wave Dispersion and Receiver Functions. *J. Asian Earth Sci.* 117, 52–63. doi:10.1016/j.jseaes.2015.12.002

Luo, T. X. (2007). The Maanshan Titanomagnetite deposit in Jinping, Yunnan. *Yunnan Geology.* 1, 124–128.

Parkhurst, D. L., and Appelo, C. A. J. (1999). User's Guide to PHREEQC (Version2)-A Computer Program for Speciation, Reaction-Path, One-Dimensional Transport, and Inverse Geochemical Calculations. USGS Water Resources Investigation Report 99-4259. Reston, Virginia: U.S. Geological Survey. doi:10.3133/wri994259

Qu, Y. H., Yuan, P. Q., and Suai, K. Y. (1998). *Potash- Forming Rules and prospect of Lower Tertiary in Lanping- Simao Basin*. Yunnan, Beijing: Geological Publishing House.

Tang, X., Zhang, J., Pang, Z., Hu, S., Tian, J., and Bao, S. (2017). The Eastern Tibetan Plateau Geothermal belt, Western China: Geology, Geophysics, Genesis, and Hydrothermal System. *Tectonophysics* 717, 433–448. doi:10.1016/j.tecto.2017.08.035

Tong, T. W., and Zhang, M. T. (1994). *Thermal Springs in Hengduan (Traverse) Mountains (In Chinese)*. Beijing: Science Pres.

Toutain, J. P., Munoz, M., Poitrasson, F., and Lienard, A. C. (1997). Springwater Chloride Ion Anomaly Prior to a ML = 5.2 Pyrenean Earthquake. *Earth Planet. Sci. Lett.* 149, 113–119. doi:10.1016/s0012-821x(97)00066-6

Tsunogai, U., and Wakita, H. (1995). Precursory Chemical Changes in Ground Water: Kobe Earthquake, Japan. *Science* 269, 61–63. doi:10.1126/science.269.5220.61

Verma, S. P., and Santoyo, E. (1997). New Improved Equations for , and SiO2 Geothermometers by Outlier Detection and Rejection. *J. Volcanology Geothermal Res.* 79, 9–23. doi:10.1016/s0377-0273(97)00024-3

Wang, J., Xiong, L., and Pang, Z. (1993). *Low-medium Temperature Convective Geothermal System (In Chinese)*. Beijing: Science Press.

Xing, L. N., Guo, H. M., Wei, L., Zhan, Y. H., Hou, C. T., Li, R. M., et al. (2012). Evolution Feature and Gensis of Fluoride Groudwater in Shallow Aquifer from north China plain (In Chinese). *J. Earth Sci. Environ.* 34 (4), 57–67.

Xu, Q., Wang, J., Wang, J., and Zhang, W. (1992). Terrestrial Heat Flow and its Tectonic Significance in Yunnan, China (In Chinese). *Geotecton Metallog* 16, 285–299.

Yang, J. W., Zhao, J. B., Zhang, P. Y., He, Y. W., Wang, J., and Cha, W. J. (2019). Forecast and Data Demonstration of the Mojiang MS5.9 Earthquake, Yunnan on September 8, 2018. *Earthquake Res. China* 35, 509–520.

Yunnan Bureau of Geology and Mineral Resources (1986). *Geology of He Saline Deposits in Simao District*. Yunnan, Beijing: Geologsical Publishing House.

Yunnan Bureau of Geology and Mineral Resources (1990). *Regional Geology of Yunnan Province*. Beijing: Geological Publishing House.

Zhang, L., Liu, Y. W., Ren, H. W., and Ke, Y. L. (2019a). Application of Hydrochemistry to the Verification of Groundwater Anomalies (In Chinese). *Earthquake* 39, 29–38. doi:10.1007/s11032-019-0984-5

Zhang, X., Fu, Z., Fu, Z., Xu, L., Li, C., and Fu, H. (2019b). The 2018 MS 5.9 Mojiang Earthquake: Source Model and Intensity Based on Near-Field Seismic Recordings. *Earth Planet. Phys.* 3 (3), 268–281. doi:10.26464/epp2019028

Zhang, Y. Q., Zhou, X., Liu, H. S., Tan, M. R., Hai, K., Yu, M. X., et al. (2018). Hydrogeological Characteristics of the hot springs and Salty Springs Occurring in the Redbeds in the Lanping-Simao Basin of Yunnan. *Hydrogeology Eng. Geology.* 45, 40–48. doi:10.16030/j.cnki.issn.1000-3665.2018.03.05

Zhang, Y. S., Gao, D. L., Shi, L., Liu, Y., Zhang, X. Y., and Li, B. L. (2013). Hydrochemical Characteristics of Salt Spring and Potassium Prospecting Research in Mengla Salt-Belts of Simao Basin, Yunnan. *J. Salt Lake Res.* 21, 10–17.

Zhang, Y., Zhou, X., Liu, H., and Fang, B. (2020a). Geochemistry of Rare Earth Elements in the hot springs in the Simao Basin in Southwestern China. *Environ. Earth Sci.* 79, 121. doi:10.1007/s12665-020-8883-y

Zhang, Y., Zhou, X., Liu, H., Yu, M., Hai, K., Tan, M., et al. (2019c). Hydrogeochemistry, Geothermometry, and Genesis of the Hot Springs in the Simao Basin in Southwestern China. *Geofluids* 2019, 1–23. doi:10.1155/2019/7046320

Zhang, Z., Yao, H., and Yang, Y. (2020b). Shear Wave Velocity Structure of the Crust and Upper Mantle in Southeastern Tibet and its Geodynamic Implications. *Sci. China Earth Sci.* 63, 1278–1293. doi:10.1007/s11430-020-9625-3

Zhao, C. P., Wang, Y., Ran, H., Zhou, Z., and Chen, Y. L. (2018). Leakage of Mantle Helium in Southwest Yunnan: Genetic Significance of M6 Earthquake Clustering in the Simao-Pu'er Seismic Zone. *Prog. Earthquake Sci.* 8, 137–139. doi:10.3969/j.issn.0253-4975.2018.08.120

Zhou, X., Jin, X., Liang, S., Shen, Y., and Zhang, H. (2017). *Special Topics on Groundwater Sciences (In Chinese)*. 2nd edn. Beijing: Geological Publishing House.

Conflict of Interest: The authors declare that the research was conducted in the absence of any commercial or financial relationships that could be construed as a potential conflict of interest.